NASA Technical Memorandum 101669

AEROBRAKING CHARACTERISTICS FOR SEVERAL POTENTIAL MANNED MARS ENTRY VEHICLES

Paul V. Tartabini and
William T. Suit

November 1989

National Aeronautics and
Space Administration

Langley Research Center
Hampton, Virginia 23665

(NASA-TM-101669) AEROBRAKING CHARACTERISTICS FOR SEVERAL POTENTIAL MANNED MARS ENTRY VEHICLES (NASA) 29 p CSCL 22B

N90-14272

Unclas

G3/18 0252604

ABSTRACT

While a reduction in weight is always desirable for any space vehicle, it is crucial for vehicles to be used in the proposed Manned Mars Mission (MMM). One such way to reduce a spacecraft's weight is through aeroassist braking which is an alternative to retro-rockets, the traditional method of slowing a craft approaching from a high energy orbit. In this paper aeroassist braking was examined for two blunt vehicle configurations and one streamlined configuration. For each vehicle type a range of L/D's was examined and the entry angle windows, bank profiles, and trajectory parameters were recorded here. In addition the sensitivities of velocity and acceleration with respect to the entry angle and bank angles were included. Also, the effect of using different atmosphere models was tested by incorporating several models into the simulation program.

INTRODUCTION

With the possibility of there being an orbiting space station capable of assembling and launching large vehicles in the near future, the enthusiasm for a manned mission to Mars is growing. Even though much fuel, and consequently weight, will be saved for such a mission by launching the spacecraft from the space station, more can be saved in the method of braking the vehicle. Traditionally retro-rockets have been used to slow a craft descending from a high energy orbit. Over the years much research has been done on aeroassist braking which can significantly increase the allowable payload weight by eliminating the need for all propulsive maneuvers (see reference 1). Most of this past research has dealt with the return to Earth leg of the trip, but further payload weight can be gained by using aerobraking at Mars as well. The purpose of this paper is to obtain an indication of the required accuracy of guidance systems for a Mars entry using the characteristics of several possible entry vehicles, and to give some insight into the braking trajectories required to obtain such accuracy.

SYMBOLS

A	area, square meters
accel.	acceleration, meters/second squared
CD	drag coefficient
CL	lift coefficient
hp_1	first pass perigee altitude, kilometers
hp_2	second pass perigee altitude, kilometers
L/D	lift to drag ratio
M	mass, kilograms

hp_2	second pass perigee altitude, km
L/D	lift- to- drag ratio
M	mass, kilograms
M/C_dA	ballistic coefficient, kilograms/meters squared
γ_i	initial flight path angle or entry angle, degrees
Δa	change in acceleration, meters/second squared
$\Delta\gamma_i$	change in entry angle, degrees
Δhp	change in perigee altitude, km
ΔV	change in velocity, meters/second

SYMBOLS FOR FIGURES

ALTITO	altitude, meters
ASMG	acceleration, g's
BNKANG	bankangle, degrees

APPROACH

The various problems studied in this paper were simulated with the use of the computer program, Program to Optimize Simulated Trajectories (POST). The same procedure was followed by POST for all of the runs mentioned unless otherwise specified. In brief, the vehicle entered the Martian atmosphere at an altitude of 300,000 m and an entry angle either chosen by POST or the user. By varying the bank angle, POST could manipulate the lift vector and , therefore, exert further control on the type of trajectory flown. A set of bank angles that would insure capture into Mars' gravitational field was chosen by the program. These bank angles were dependent upon the entry flight path angle and a number of possible constraints placed on the trajectory by the user. If the constraints along with the initial flight path angle were not conflicting or unreasonable, a suitable trajectory resulting in capture and conforming to the user defined constraints occurred. If, however, POST could not handle the constraints, usually because they conflicted with each other, a crash or skip out would result. For the simulations done in this study constraints were placed on acceleration, altitude, and velocity. Acceleration was constrained to an upper bound limit of 5 g's . Altitude had a lower bound limit of 32,000 m to insure avoidance of terrain on Mars that extend to heights of 28 to 30 km, and the velocity was targeted to a value of 4700 m/s in order to secure capture which occurs at a velocity near 5000 m/s. The user was free to change any of the constraints by manipulating the dependent variables. As long as a variable was dependent on the control variables, which in these cases were the entry flight path angle and the bank angle, it could be used to constrain the vehicle.

The first part of the study dealt primarily with finding the entry flight path angle window for a range of potential manned Mars vehicles in two basic categories: blunt and streamlined. The physical and aerodynamic characteristics for these vehicles are listed in Table 1. For each of these two categories a range of lift- to- drag ratios were tested. The L/D's were altered by changing the lift coefficient which represented a change in the shape of the vehicle. To determine the window, maximum and minimum entry flight path angles that would result in capture were determined by POST along with the corresponding bank angles. The difference between the maximum and minimum flight path angle was the desired window. Also, the effect of minimizing the number of bank angles and thus conserving fuel used for the reaction control system (RCS) was examined.

After these windows were determined, a simulation was run with a fixed entry angle located in the middle of the window. When this intermediate entry angle along with its corresponding bank angles achieved capture it was varied by $\pm 0.001^{\circ}$ while maintaining the same bank angles to test the sensitivity to velocity, acceleration, and altitude at the first pass perigee. Similar sensitivity tests were conducted on the bank angles.

The final part of the study dealt with models of different atmospheres. The original model, and the one used most often in this study, was developed by The Committee on Space Research (COSPAR) and is called the COSPAR model. Three other models were chosen to obtain an idea of the sensitivity of the guidance system to the type of atmosphere. The first was a revised COSPAR model. The other two were models in which the lower atmospheric data was provided by the Viking Landers, and the upper atmospheric data was generated by a computer program. The combined data included a model of a summer morning with low dust content and a winter morning with medium dust content. These Martian atmosphere models were obtained from an unpublished paper written by David Pitts and others from NASA's Johnson Space Center.

RESULTS & DISCUSSION

Similar entry studies conducted in the past indicated that constrained capture trajectories flown at a constant bank angle were very sensitive to the entry flight path angle (reference 2). Variations as small as 0.0001° would considerably alter the trajectory parameters. Therefore our studies allowed POST to change the bank angles up to sixteen times for each run. This enabled it to find a suitable bank angle profile that, combined with the entry angle, resulted in a successful trajectory.

The characteristics of the two blunt vehicle configurations are given in Table 1. A majority of the research was conducted with the vehicle with the larger ballistic coefficient since a drag coefficient of 1.35 is a fairly realistic value and also because there was unpublished aerodynamic data compiled for that type of vehicle. Entry angle windows were determined for lift-to-drag ratios of 0.3, 0.5, 0.75 and 1.0. Generally, the windows widened as the L/D increased since a higher L/D resulted in greater lift and therefore control. Although the windows increased with the L/D, the corresponding increases seemed to lessen as the L/D increased. Also, the window appeared to widen as the ballistic coefficient increased, although this increase is less obvious in the lower L/D configurations. The magnitudes of these windows along with the values of the maximum and minimum entry angles are displayed in Table 2.

The trajectories for a typical maximum flight path angle stayed higher in the atmosphere for a longer period of time than the minimum flight path angles. For a period of 700 to 800 sa vehicle flying a maximum initial flight path angle flew a bank angle profile that tended towards 180^{o} (full lift down). This was favored in order to hold the vehicle in the atmosphere and avoid a skip-out. Minimum flight path angle trajectories, on the other hand, favored a 0^{o} bank profile (full lift up) for 500 to 600 s in order to keep the spacecraft from crashing into the planet's surface. Time histories for a typical maximum and minimum run are shown in figures 1 and 2, respectively. Table 3 includes listings of the bankangles for each run made. All table entries are for sixteen step bank profiles unless otherwise noted. Also, Table 4 includes a list of the maximum acceleration and heat rate in order to give the reader an idea of the magnitudes of those parameters.

As previously mentioned, the sensitivity of velocity, acceleration, and altitude to the entry flight path angle was tested for each vehicle configuration by varying an entry angle located in the middle its window by ±0.001^{o}. The relevant sensitivities (see Table 5) were examined at perigee in this manner since POST calculated them for these parameters only at the end of the trajectory. From the table it can be seen that a small change in the initial flight path angle can bring about immense changes in the velocity and acceleration of the vehicle and somewhat larger changes in altitude. The sensitivity of these parameters were also looked at with respect to the bankangles. Table 3 has the bank sensitivities with respect to velocity and acceleration listed for all of the runs made. On several runs the sensitivity with respect to altitude is also listed. It can be seen that the trajectory is not overly sensitive to any one bank angle. The acceleration is virtually independent of the bank angle, its sensitivity being either zero or very minute. The sensitivity to velocity is also small except for several of the higher L/D vehicles. The most sensitive angles appear in the region where acceleration and lift are highest since this is where the most control can be gained (see figures 1 and 2). Although one bank angle alone may not be that sensitive, if several are changed in this high control region, the velocity can change noticeably.

As is evident from figures 1 & 2, the bank profiles require almost a constant firing of the RCS, and the changes in bank required are relatively large. In order to reduce the amount of fuel needed for the RCS, bank angle profiles with less dramatic changes were examined. As a vehicle flies through a trajectory, POST continually alters the bank angle to control it. The trajectory can be divided into a specified number of steps defined by the user. For each of these steps POST tries to find one bank angle that will successfully meet the trajectory constraints. Therefore, by having many steps more control can be gained. For most of the runs the bank angles were allowed to change sixteen to nineteen times. These runs resulted in widely changing but successful bank profiles. In an effort to minimize the amount of use of the RCS, the number of steps was cut down to as far as two. Figures 3-a and 3-b show minimum runs for the same vehicle. Figure3-a has a sixteen step bank profile, and figure 3-b has a two step profile. In figure 3-a the magnitudes of the changes in bank are almost 200^{o} . In figure 3-b the bank angle is constantly changing, but it only goes as high as 0.4^{o}. Also, the perigee conditions listed at the top of both figures indicate that the runs are relatively the same except for their bank profiles. This fact suggests that there is more than one way to fly these trajectories. Although it seemed as though the number of steps could be reduced on any run, the maximum flight path angle runs were more difficult to scale down. They often required at least five steps to allow POST to change the bank angle, but once a suitable profile was found it resulted in trajectory parameters much like the many step maximum flight path angle runs.

The next part of the study dealt with a more streamlined vehicle with a larger ballistic coefficient of 2970.7 kg/m^2 (see Table 1). As with the blunt configurations, entry windows were determined for L/D's of 0.5, 0.75, and 1.0. The tests for this vehicle class were run in the same general way. Less changes were made in the bank profile, with most vehicles flying a constant full lift up or down trajectory. The same constraints were utilized, but for this vehicle the altitude constraint of 32 km seemed too stringent, and meeting it resulted in windows of only 0.65^{o} to 0.90^{o} wide. Flying full lift down for maximum runs and full lift up for minimum runs made windows as large as 4.2^{o} possible, but for the minimum runs the perigee altitudes were considerably lower than the desired 32 km and the acceleration rates were much larger than 5 g's. These results are outlined in Table 6 which contains data from four different runs for each L/D. Four runs were used to show the change in the entry flight path angle window as various constraints were met. The windows, perigee altitudes, and maximum acceleration rates were calculated for a maximum run and minimum runs that met the 32 km perigee constraint and the 5 g acceleration constraint. For comparison, an arbitrarily chosen 12 km perigee constraint was also run. Like the runs for the blunter configurations, the windows increased with the L/D with the increases leveling off as the L/D's got higher. The 32 km perigee limit seemed to be the constraint that reduced the window the most, with a larger window attainable with the 5 g acceleration constraint. Table 4 contains the maximum acceleration and heat rates for the vehicles of this class.

Sensitivities of velocity, acceleration, and altitude at perigee were examined in the same manner as for the blunt configurations. This vehicle proved to be much more sensitive to changes in the initial entry angle (see Table 5). The bank sensitivities were also calculated for this vehicle, and are listed in Table 3. They are similar in magnitude to the ones for the blunter vehicle configurations.

Earlier it was mentioned that the type of trajectory flown could be influenced by certain user defined constraints placed on the vehicle and trajectory. These constraints should be realistic in that an actual guidance system should be able to target the certain variables. For example, the projected perigee altitude (ALTP) constraint, although helpful in establishing a successful orbit, would be difficult to enforce in a real situation. The best constraints seemed to be the ones on velocity, acceleration, and altitude. Several runs were made with different combinations of these three variables, all of which included velocity and at least one of the other two variables. These runs all yielded the same end results and sensitivities, indicating that there is some versatility in choosing a guidance system to perform this job. Furthermore, the constraints are realistic since guidance systems in existence today have the capability to target these variables (see reference 3).

On most of the minimum runs the projected second pass perigee altitude was lower than the preferred 32 km , sometimes even crashing into the surface. Although it is still unknown as to whether or not the vehicle will need to make a second pass through the atmosphere, the ways in achieving it were examined. In order to change the orbit, the vehicle must undergo a certain change in velocity. With the aid of POST, these velocity changes were simulated at apogee of the captured orbit and their magnitudes were determined (see Table 7). Clearly these velocity changes are small and indicate that an unsatisfactory projected second pass perigee altitude would not be a difficult problem to remedy in an actual situation.

The different atmospheric models were the final topic examined in this study. As previously mentioned, there were three other models in addition to the COSPAR model which was used for the bulk of the research. Table 8 describes the density characteristics for all four of these models. These density profiles were taken from unpublished data by David Pitts ,et al and is included here for the convenience of the reader. The models were only used on maximum runs since these seemed to be the most sensitive and stayed in the atmosphere the longest. Table 9 lists the maximum entry angle, altitude at perigee and the maximum acceleration and heating rates for runs in all four atmospheres. It can be seen that there is not much of a difference between the results for each of these different atmospheres suggesting that the type of atmosphere makes little difference in the end results of the trajectory.

CONCLUSION

For the blunt vehicle configurations, entry angle windows of 1^{o} to 1.5^{o} were possible, although these trajectories were somewhat sensitive to changes in initial flight path angle and bank angle. The streamlined vehicle that was studied showed a possibility for adequate entry angle windows if the constraints placed on it were not too demanding. This vehicle proved to be even more sensitive to changes in entry and bank angles than the blunt configurations. It was also shown that many changes in bank angle are not required to obtain a suitable trajectory, thus enabling the amount of use of the reaction control system to be minimized. Also, the magnitudes of the velocity changes needed to change the second pass perigee altitude were calculated and turned out to be very small. Finally, four different atmospheric models were used to determine the effect of the atmosphere type on the trajectory. There were virtually no differences between runs using each model.

REFERENCES

1. Walberg, Gerald D.: "A Review of Aeroassisted Orbital Transfer", AIAA Paper No. 82-1378, AIAA 9th Atmospheric Flight Mechanics Conference, San Diego, CA, August 1982.

2. Lee, Mary Chloe, and Suit, William T.: "Preliminary Investigation of Parameter Sensitivities for Atmospheric Entry and Aerobraking at Mars", NASA TM-101607, September 1989.

3. Gamble, J.D.; Cerimele, C.J.; Moore, T.E.; and Higgins, J.: "Atmospheric Guidance Concepts for an Aeroassist Flight Experiment", Journal of the Astronautical Sciences, 1988.

Table 1. Vehicle Characteristics

Blunt Vehicles	
Vehicle Type 1	$M = 226,378$ kg $M/C_DA = 919.3$ kg/m^2 $A = 182.415$ m^2 $C_D = 1.35$
Vehicle Type 2	$M = 226,378$ kg $M/C_DA = 620.5$ kg/m^2 $A = 182.415$ m^2 $C_D = 2$
Streamlined Vehicle	
Vehicle Type 1	$M = 136,116.2$ kg $M/C_DA = 2970.7$ kg/m^2 $A = 79$ m^2 $C_D = 0.58845$

Table 2. Entry Angle Windows for Blunt Vehicles

L/D	M/C_DA (kg/m^2)	C_D	Max γ_i	Min γ_i	$\Delta\gamma_i$
0.3	620.5	2	−18.3193°	−19.1109°	0.7916°
0.3	919.3	1.35	−18.4461°	−19.2344°	0.7883°
0.5	620.5	2	−18.2415°	−19.5880°	1.3465°
0.5	919.3	1.35	−18.3289°	−19.7263°	1.3974°
0.75	919.3	1.35	−18.2432°	−20.0423°	1.7991°
1.0	620.5	2	−18.0646°	−19.6747°	1.6101°
1.0	919.3	1.35	−18.3492°	−20.2000°	1.8508°

Table 3. Bank Angles and Bank Sensitivities

	Time								
	0 to 197	197 to 225	225 to 240	240 to 250	250 to 270	270 to 280	280 to 290	290 to 305	305 to end
$L/D = 0.3$; $C_D = 1.35$; $M/C_DA = 919.3$; Maximum Flight Path Angle									
ϕ	200	188	134	130	96	70	65	187	180
$\Delta V/\Delta\phi$	-2.78	-0.69	-4.94	-6.14	-4.78	-2.01	-1.27	-0.23	0
$\Delta a/\Delta\phi$	0.02	0	0.03	0.01	0	0	0	0	0
$L/D = 0.3$; $C_D = 1.35$; $M/C_DA = 919.3$; Minimum Flight Path Angle									
ϕ	1	-6	4	51	59	179	180	180	180
$\Delta V/\Delta\phi$	-0.03	-0.06	-0.27	-0.14	-0.04	0	0	0	0
$\Delta a/\Delta\phi$	0	0	0	0	0	0	0	0	0
$L/D = 0.5$; $C_D = 1.35$; $M/C_DA = 919.3$; Maximum Flight Path Angle									
ϕ	184	184	136	136	102	73	67	190	180
$\Delta V/\Delta\phi$	0.65	0.68	-10.43	-13.46	-11.17	-5.43	-3.50	-0.63	0
$\Delta a/\Delta\phi$	-0.01	-0.01	-0.07	-0.06	-0.01	0	0	0	0
$L/D = 0.5$; $C_D = 1.35$; $M/C_DA = 919.3$; Minimum Flight Path Angle									
ϕ	1	0	16	50	59	60	60	179	180
$\Delta V/\Delta\phi$	-0.02	0.03	-0.02	0	0	0	0	0	0
$\Delta a/\Delta\phi$	0	0	0	0	0	0	0	0	0
$L/D = 0.75$; $C_D = 1.35$; $M/C_DA = 919.3$; Maximum Flight Path Angle									
ϕ	169	181	123	125	92	72	67	190	180
$\Delta V/\Delta\phi$	6.28	4.54	-21.18	-29.66	-26.20	-13.82	-9.19	-1.71	0
$\Delta a/\Delta\phi$	0	0	0	0	0	0	0	0	0

Table 3. Continued

	Time								
	0 to 125	125 to 200	200 to 250	250 to 300	300 to end				
$L/D = 0.75$; $C_D = 1.35$; $M/C_DA = 919.3$; Minimum Flight Path Angle (5 steps)									
ϕ	48	−67	−8	0	0				
$\Delta V/\Delta\phi$	3.78	12.30	−0.24	0	0				
$\Delta h/\Delta\phi$	13.15	24.04	0	0	0				
$\Delta a/\Delta\phi$	−0.03	−0.06	0	0	0				
$L/D = 1.0$; $C_D = 1.35$; $M/C_DA = 919.3$; Maximum Flight Path Angle									
ϕ	104	179	103	101	82	66	63	183	180
$\Delta V/\Delta\phi$	−151.38	−43.30	−49.49	−68.96	−65.19	−35.92	−23.79	−4.59	0
$\Delta a/\Delta\phi$	0	0	0	0	0	0	0	0	0
	Time								
	0 to 100	100 to 176	176 to 206	206 to end					
$L/D = 1.0$; $C_D = 1.35$; $M/C_DA = 919.3$; Minimum Flight Path Angle (4 steps)									
ϕ	0	0	75	180					
$\Delta V/\Delta\phi$	NA								
$\Delta a/\Delta\phi$	NA								
	Time								
	0 to 197	197 to 225	225 to 240	240 to 250	250 to 270	270 to 280	280 to 290	290 to 305	305 to end
$L/D = 0.3$; $C_D = 2.0$; $M/C_DA = 620.5$; Maximum Flight Path Angle									
ϕ	200	187	135	130	96	70	65	187	180
$\Delta V/\Delta\phi$	−2.59	−0.58	−4.77	−5.99	−4.64	−2.02	−1.21	−0.21	0
$\Delta a/\Delta\phi$	0	0	0	0	0	0	0	0	0

Table 3. Continued

	Time								
	0 to 125	125 to 200	200 to 250	250 to 300	300 to end				
$L/D = 0.3$; $C_D = 2.0$; $M/C_DA = 620.5$; Minimum Flight Path Angle									
ϕ	1	6	–1	33	52	59	60	179	180
$\Delta V/\Delta\phi$	0	0	0.02	–0.30	–0.80	–0.39	–0.15	–0.03	0
$\Delta a/\Delta\phi$	0	0	0	0	0	0	0	0	0
$L/D = 0.5$; $C_D = 2.0$; $M/C_DA = 620.5$; Maximum Flight Path Angle									
ϕ	223	196	122	119	91	69	64	186	180
$\Delta V/\Delta\phi$	35.78	11.29	–16.59	–23.76	–20.87	–10.89	–7.48	–1.35	0
$\Delta a/\Delta\phi$	0	0	0	0	0	0	0	0	0
$L/D = 0.5$; $C_D = 2.0$; $M/C_DA = 620.5$; Minimum Flight Path Angle									
ϕ	1	0	20	52	59	60	60	179	180
$\Delta V/\Delta\phi$	0	0.03	–0.02	0	0	0	0	0	0
$\Delta a/\Delta\phi$	0	0	0	0	0	0	0	0	0
$L/D = 1.0$; $C_D = 2.0$; $M/C_DA = 620.5$; Maximum Flight Path Angle									
ϕ	194	195	110	110	88	68	64	185	180
$\Delta V/\Delta\phi$	11.46	8.53	–43.79	–64.32	–62.23	–36.10	–24.61	–4.37	0
$\Delta a/\Delta\phi$	–0.05	–0.04	–0.17	–0.18	–0.06	0	0	0	0

Table 3. Continued

	Time								
	0 to 197	197 to 225	225 to 240	240 to 250	250 to 270	270 to 280	280 to 290	290 to 305	305 to end
$L/D = 1.0$; $C_D = 2.0$; $M/C_DA = 620.5$; Maximum Flight Path Angle									
ϕ	54	266	56	53	58	60	60	180	180
$\Delta V/\Delta\phi$	-60.16	0.23	-0.50	-0.30	-0.09	-0.01	0	0	0
$\Delta h/\Delta\phi$	-104.39	0	0	0	0	0	0	0	0
$\Delta a/\Delta\phi$	0.36	0	0	0	0	0	0	0	0
$L/D = 0.5$; $C_D = 0.59$; $M/C_DA = 2970.7$; Maximum Flight Path Angle									
ϕ	180	180	180	180	180	180	180	180	180
$\Delta V/\Delta\phi$	-15.08	0.72	0.46	1.28	-0.07	0.01	0.01	0	0
$\Delta h/\Delta\phi$	0	0	0	0	0	0	0	0	0
$\Delta a/\Delta\phi$	0.02	0	0	0	0	0	0	0	0
$L/D = 0.5$; $C_D = 0.59$; $M/C_DA = 2970.7$; Minimum Flight Path Angle									
ϕ	4	10	10	10	10	10	10	10	10
$\Delta V/\Delta\phi$	-1.46	-0.01	0	0	0	0	0	0	0
$\Delta a/\Delta\phi$	0.02	0	0	0	0	0	0	0	0
	Time								
	0 to 125	125 to 200	200 to 230	230 to 260	260 to 430	430 to end			
$L/D = 0.75$; $C_D = 0.59$; $M/C_DA = 2970.7$; Maximum Flight Path Angle (6 steps)									
ϕ	180	180	180	180	180	180			
$\Delta V/\Delta\phi$	1.38	4.57	3.42	-1.21	2.94	0			
$\Delta h/\Delta\phi$	0.59	2.04	1.63	-0.34	-0.14	0			
$\Delta a/\Delta\phi$	0	0	0	0	0	0			
	Time								
	0 to 125	125 to 200	200 to 225	225 to 300	300 to end				
$L/D = 0.75$; $C_D = 0.59$; $M/C_DA = 2970.7$; Minimum Flight Path Angle (5 steps)									
$\Delta V/\Delta\phi$	-2.32	-10.30	-0.38	0	0				
$\Delta a/\Delta\phi$	0.01	0.06	0	0	0				

Table 3. Continued

	Time								
	0 to 75	75 to 200	200 to 230	230 to 260	260 to 430	430 to end			
$L/D = 1.0$; $C_D = 0.59$; $M/C_DA = 2970.7$; Maximum Flight Path Angle (6 steps)									
ϕ	180	180	180	180	180	180			
$\Delta V/\Delta\phi$	−0.67	−9.77	−6.67	−4.99	1.15	0			
$\Delta h/\Delta\phi$	−0.09	−1.23	−0.74	−0.20	−0.04	0			
$\Delta a/\Delta\phi$	0	0	0	0	0	0			
	Time								
	0 to 125	125 to 170	170 to 200	200 to 250	250 to end				
$L/D = 1.0$; $C_D = 0.59$; $M/C_DA = 2970.7$; Minimum Flight Path Angle (5 steps)									
ϕ	1	28	98	15	10				
$\Delta V/\Delta\phi$	−1.44	−20.11	−16.77	−0.99	0				
$\Delta a/\Delta\phi$	0.04	0.27	0.03	0	0				
	Time								
	0 to 197	197 to 225	225 to 240	240 to 250	250 to 270	270 to 280	280 to 290	290 to 305	305 to end
$L/D = 0.3$; $C_D = 1.35$; $M/C_DA = 919.3$; Maximum Flight Path Angle (Revised COSPAR atmosphere)									
ϕ	200	187	132	128	95	70	65	187	180
$\Delta V/\Delta\phi$	−2.56	−0.53	−4.58	−5.71	−4.41	−1.93	−1.18	−0.21	0
$\Delta a/\Delta\phi$	−0.02	0	−0.02	0.01	0	0	0	0	0
$L/D = 0.3$; $C_D = 1.35$; $M/C_DA = 919.3$; Maximum Flight Path Angle (Summer morning low-dust atmosphere)									
ϕ	200	188	131	126	93	69	65	186	180
$\Delta V/\Delta\phi$	−3.83	−0.99	−5.11	−6.15	−4.62	−1.98	−1.23	−0.22	0
$\Delta a/\Delta\phi$	0	0.03	0	0.03	0.02	0	0	0	0

Table 3. Continued

	Time								
	0 to 197	197 to 225	225 to 240	240 to 250	250 to 270	270 to 280	280 to 290	290 to 305	305 to end
$L/D = 0.3$; $C_D = 1.35$; $M/C_DA = 919.3$; Maximum Flight Path Angle (Winter morning medium-dust atmosphere)									
ϕ	201	189	132	126	93	69	65	186	180
$\Delta V/\Delta\phi$	−4.02	−1.05	−5.16	−6.23	−4.67	−1.99	−1.22	−0.22	0
$\Delta a/\Delta\phi$	0.04	0.01	0.03	0.02	0	0	0	0	0
$L/D = 0.3$; $C_D = 2.0$; $M/C_DA = 620.5$; Maximum Flight Path Angle (Revised COSPAR atmosphere)									
ϕ	190	187	123	121	93	70	65	187	180
$\Delta V/\Delta\phi$	−2.89	−0.59	−4.64	−5.50	−3.97	−1.66	−1.00	−0.19	0
$\Delta a/\Delta\phi$	0	0	0	0	0	0	0	0	0
$L/D = 0.3$; $C_D = 2.0$; $M/C_DA = 620.5$; Maximum Flight Path Angle (Summer morning low-dust atmosphere)									
ϕ	199	188	132	127	94	69	65	186	180
$\Delta V/\Delta\phi$	−2.67	−0.61	−4.95	−6.10	−4.59	−1.92	−1.14	−0.21	0
$\Delta a/\Delta\phi$	0	0	0	0	0	0	0	0	0
$L/D = 0.3$; $C_D = 2.0$; $M/C_DA = 620.5$; Maximum Flight Path Angle (Winter morning medium-dust atmosphere)									
ϕ	199	188	132	127	93	69	65	186	180
$\Delta V/\Delta\phi$	−2.76	−0.64	−5.03	−6.18	−4.62	−1.92	−1.13	−0.21	0
$\Delta a/\Delta\phi$	0	0	0	0	0	0	0	0	0

Table 3. Concluded

	Time								
	0 to 197	197 to 225	225 to 240	240 to 250	250 to 270	270 to 280	280 to 290	290 to 305	305 to end
$L/D = 0.5$; $C_D = 1.35$; $M/C_DA = 919.3$; Maximum Flight Path Angle (Revised COSPAR atmosphere)									
ϕ	190	187	123	121	93	70	65	187	180
$\Delta V/\Delta\phi$	23.83	7.02	−10.36	−14.17	−11.92	−5.91	−3.90	−0.68	0
$\Delta a/\Delta\phi$	−0.14	−0.04	−0.05	−0.04	−0.01	0	0	0	0
$L/D = 0.5$; $C_D = 1.35$; $M/C_DA = 919.3$; Maximum Flight Path Angle (Summer morning low-dust atmosphere)									
ϕ	157	181	117	113	88	68	64	185	180
$\Delta V/\Delta\phi$	−17.78	−5.05	−10.44	−12.91	−10.17	−4.73	−3.05	−0.57	0
$\Delta a/\Delta\phi$	0	0	0	0	0	0	0	0	0
$L/D = 0.5$; $C_D = 1.35$; $M/C_DA = 919.3$; Maximum Flight Path Angle (Winter morning medium-dust atmosphere)									
ϕ	157	181	117	113	88	68	64	185	180
$\Delta V/\Delta\phi$	−17.86	−5.08	−10.47	−12.94	−10.15	−4.68	−3.00	−0.56	0
$\Delta a/\Delta\phi$	0	0	0	0	0	0	0	0	0

Table 4. Maximum Acceleration and Heating Rates for All Vehicles

M/C_DA(kg/m^2)	C_D	L/D	Opt. Type	Maximum Accel. (m/s^2)	Maximum Heat Rt. (BTU/ft^{2}s)	Maximum Heat Rt. (W/m^2)
919.3	1.35	0.3	Max	18.7	118.1	1.34×10^6
919.3	1.35	0.3	Min	32.2	156.5	1.78×10^6
919.3	1.35	0.5	Max	18.7	113.8	1.29×10^6
919.3	1.35	0.5	Min	42.7	173.8	1.97×10^6
919.3	1.35	0.75	Max	19.8	112.0	1.27×10^6
919.3	1.35	0.75	Min	49.4	175.4	1.99×10^6
919.3	1.35	1.0	Max	27.8	119.0	1.35×10^6
919.3	1.35	1.0	Min	49.5	174.4	1.98×10^6
620.5	2.00	0.3	Max	18.8	97.6	1.11×10^6
620.5	2.00	0.3	Min	32.8	130.4	1.48×10^6
620.5	2.00	0.5	Max	20.3	95.9	1.09×10^6
620.5	2.00	0.5	Min	42.1	144.9	1.64×10^6
2970.7	0.59	0.5	Max	12.5	178.0	2.02×10^6
2970.7	0.59	0.5	Min	51.0	326.9	3.71×10^6
2970.7	0.59	0.75	Max	10.8	162.3	1.84×10^6
2970.7	0.59	0.75	Min	49.8	325.3	3.69×10^6
2970.7	0.59	1.0	Max	10.0	148.2	1.68×10^6
2970.7	0.59	1.0	Min	48.6	307.8	3.49×10^6

Table 5. Sensitivity of γ_i to Velocity, Altitude, and Acceleration at Perigee

L/D	M/C_DA (kg/m^2)	$\Delta\gamma_i$ (deg)	$\Delta V/\Delta\gamma_i$(m/s/deg)	$\frac{\Delta h}{\Delta\gamma_i}$ (m/deg)	$\frac{\Delta a}{\Delta\gamma_i}$ (m/s^2/deg)
0.3	919.3	+0.001	2.0×10^3	2.44×10^4	45.5
0.3	919.3	−0.001	2.0×10^3	2.38×10^4	44.6
0.5	919.3	+0.001	1.5×10^3	1.30×10^4	31.0
0.5	919.3	−0.001	1.5×10^3	1.20×10^4	29.5
0.75	919.3	+0.001	1.1×10^3	9.80×10^3	32.2
0.75	919.3	−0.001	1.1×10^3	9.80×10^3	31.7
1.0	919.3	+0.001	1.2×10^3	1.26×10^4	36.0
1.0	919.3	−0.001	1.2×10^3	1.26×10^4	36.0
0.5	2970.7	+0.001	2.3×10^3	2.84×10^4	43.3
0.5	2970.7	−0.001	2.3×10^3	2.86×10^4	86.5
0.75	2970.7	+0.001	3.8×10^3	7.33×10^4	48.8
0.75	2970.7	−0.001	3.8×10^3	7.63×10^4	48.8
1.0	2970.7	+0.001	3.1×10^3	6.09×10^4	52.8
1.0	2970.7	−0.001	3.1×10^3	1.23×10^5	53.0

Table 6. Entry Angle Windows for Streamlined Vehicle Configurations

L/D	Opt. Type	h_{p1} (km)	α_m (m/s^2)	γ_i (degrees)	Comments	$\Delta\gamma_i$ (degrees)
0.5	Max	33.0	12.5	−18.6371	Full lift down	—
0.5	Min	30.0	18.3	−19.3000	32 km constraint	0.6629
0.5	Min	17.6	51.0	−20.5083	Accel. constraint	1.8712
0.5	Min	12.3	73.4	−21.4000	12 km constraint	2.7629
0.75	Max	35.6	10.8	−18.5129	Full lift down	—
0.75	Min	32.1	17.0	−19.1970	32 km constraint	0.6841
0.75	Min	19.6	49.8	−20.6320	Accel. constraint	2.1191
0.75	Min	13.3	81.3	−22.0000	12 km constraint	3.4871
1.0	Max	37.9	10.0	−18.4240	Full lift down	—
1.0	Min	32.1	19.6	−19.3140	32 km constraint	0.8900
1.0	Min	21.8	48.6	−20.5384	Accel. constraint	2.1144
1.0	Min	13.6	93.3	−22.6500	12 km constraint	4.2260

Table 7. Necessary ΔV Needed to Achieve Desired 2nd Pass Perigee Altitude

M/C_DA (kg/m^2)	L/D	C_D	ALTP (original) (km)	ALTP (corrected) (km)	ΔV (m/s)
919.3	0.3	1.35	18.0	34.6	0.5
919.3	0.5	1.35	−3.2	34.7	1.1
620.5	0.3	2.0	21.3	33.9	0.4
620.5	0.5	2.0	1.2	33.6	0.8

Table 8a. Atmosphere—Original COSPAR

Altitude ($\times 10^3$ ft.)	Density (kg/m^3)	Altitude ($\times 10^3$ ft.)	Density (kg/m^3)
0	1.55×10^{-2}	110	4.44×10^{-8}
5	9.91×10^{-3}	120	1.00×10^{-8}
10	6.47×10^{-3}	130	2.62×10^{-9}
15	4.17×10^{-3}	140	7.89×10^{-10}
20	2.63×10^{-3}	150	2.72×10^{-10}
25	1.62×10^{-3}	160	1.20×10^{-10}
30	9.80×10^{-4}	170	5.37×10^{-11}
35	5.82×10^{-4}	180	2.43×10^{-11}
40	3.40×10^{-4}	190	1.11×10^{-11}
45	1.94×10^{-4}	200	5.15×10^{-12}
50	1.08×10^{-4}	210	2.43×10^{-12}
55	5.92×10^{-5}	220	1.15×10^{-12}
60	3.19×10^{-5}	230	5.48×10^{-13}
65	1.08×10^{-5}	240	2.62×10^{-13}
70	8.73×10^{-6}	250	1.26×10^{-13}
75	4.48×10^{-6}	260	6.05×10^{-14}
80	2.29×10^{-6}	270	2.93×10^{-14}
85	1.17×10^{-6}	280	1.42×10^{-14}
90	6.02×10^{-7}	290	6.93×10^{-15}
95	3.09×10^{-7}	300	3.39×10^{-15}
100	1.59×10^{-7}		

Table 8b. Atmosphere—Revised COSPAR

Altitude ($\times 10^3$ ft.)	Density (kg/m^3)	Altitude ($\times 10^3$ ft.)	Density (kg/m^3)
0	1.82×10^{-2}	110	1.06×10^{-7}
5	1.19×10^{-2}	120	3.31×10^{-8}
10	7.89×10^{-3}	130	1.13×10^{-8}
15	5.18×10^{-3}	140	4.18×10^{-9}
20	3.35×10^{-3}	150	1.25×10^{-9}
25	2.11×10^{-3}	160	5.65×10^{-10}
30	1.31×10^{-3}	170	3.29×10^{-10}
35	8.04×10^{-4}	180	2.14×10^{-10}
40	4.87×10^{-4}	190	1.49×10^{-10}
45	2.86×10^{-4}	200	1.07×10^{-10}
50	1.66×10^{-4}	210	7.89×10^{-11}
55	9.40×10^{-5}	220	5.89×10^{-11}
60	5.26×10^{-5}	230	4.43×10^{-11}
65	2.89×10^{-5}	240	3.36×10^{-11}
70	1.57×10^{-5}	250	2.57×10^{-11}
75	8.41×10^{-6}	260	1.97×10^{-11}
80	4.50×10^{-6}	270	1.52×10^{-11}
85	2.41×10^{-6}	280	1.19×10^{-11}
90	1.29×10^{-6}	290	9.32×10^{-12}
95	6.95×10^{-7}	300	7.37×10^{-12}
100	3.75×10^{-7}		

ORIGINAL PAGE IS
OF POOR QUALITY

Table 8c. Atmosphere—Viking I Lander
Summer Morning Low Dust Content

Altitude (× 10^3 ft.)	Density (kg/m^3)	Altitude (× 10^3 ft.)	Density (kg/m^3)
0	2.04×10^{-2}	110	3.64×10^{-8}
5	1.22×10^{-2}	120	9.23×10^{-9}
10	7.88×10^{-3}	130	2.46×10^{-9}
15	4.98×10^{-3}	140	8.35×10^{-10}
20	3.09×10^{-3}	150	3.55×10^{-10}
25	1.88×10^{-3}	160	1.68×10^{-10}
30	1.13×10^{-3}	170	8.40×10^{-11}
35	6.65×10^{-4}	180	4.39×10^{-11}
40	3.85×10^{-4}	190	2.39×10^{-11}
45	2.20×10^{-4}	200	1.34×10^{-11}
50	1.22×10^{-4}	210	7.61×10^{-12}
55	6.65×10^{-5}	220	4.43×10^{-12}
60	3.55×10^{-5}	230	2.71×10^{-12}
65	1.87×10^{-5}	240	1.72×10^{-12}
70	9.69×10^{-6}	250	1.14×10^{-12}
75	4.99×10^{-6}	260	7.66×10^{-13}
80	2.54×10^{-6}	270	5.29×10^{-13}
85	1.29×10^{-6}	280	3.76×10^{-13}
90	6.47×10^{-7}	290	2.73×10^{-13}
95	3.23×10^{-7}	300	2.03×10^{-13}
100	1.60×10^{-7}		

Table 8d. Atmosphere—Viking I

Winter Morning Medium Dust Content

Altitude ($\times 10^3$ ft.)	Density (kg/m^3)	Altitude ($\times 10^3$ ft.)	Density (kg/m^3)
0	2.64×10^{-2}	110	3.95×10^{-8}
5	1.43×10^{-2}	120	1.10×10^{-8}
10	8.83×10^{-3}	130	3.54×10^{-9}
15	5.39×10^{-3}	140	1.13×10^{-9}
20	3.27×10^{-3}	150	5.07×10^{-10}
25	1.96×10^{-3}	160	2.63×10^{-10}
30	1.16×10^{-3}	170	1.48×10^{-10}
35	6.74×10^{-4}	180	8.70×10^{-11}
40	3.88×10^{-4}	190	5.25×10^{-11}
45	2.18×10^{-4}	200	3.24×10^{-11}
50	1.21×10^{-4}	210	2.04×10^{-11}
55	6.54×10^{-5}	220	1.31×10^{-11}
60	3.48×10^{-5}	230	8.40×10^{-12}
65	1.83×10^{-5}	240	5.53×10^{-12}
70	9.50×10^{-6}	250	3.73×10^{-12}
75	4.89×10^{-6}	260	2.57×10^{-12}
80	2.50×10^{-6}	270	1.80×10^{-12}
85	1.26×10^{-6}	280	1.26×10^{-12}
90	6.36×10^{-7}	290	9.07×10^{-13}
95	3.20×10^{-7}	300	6.65×10^{-13}
100	1.62×10^{-7}		

Table 9. Effects of Different Atmosphere Models

M/C_DA (kg/m^2)	C_D	L/D	Atmosphere Model Type	h_{p1} (km)	h_{p2} (km)	Max γ_i
919.3	1.35	0.3	COSPAR	43.8	38.7	–18.4461°
919.3	1.35	0.3	Revised COSPAR	42.2	47.4	–18.3105°
919.3	1.35	0.3	Viking I, Summer, Morning, Low Dust	44.6	39.7	–18.4096°
919.3	1.35	0.3	Viking I, Winter, Morning, Medium Dust	39.7	44.6	–18.4109°
919.3	1.35	0.5	COSPAR	39.2	49.9	–18.3289°
919.3	1.35	0.5	Revised COSPAR	42.5	52.5	–18.2040°
919.3	1.35	0.5	Viking I, Summer, Morning, Low Dust	39.5	50.0	–18.3326°
919.3	1.35	0.5	Viking I, Winter, Morning, Medium Dust	39.5	48.8	–18.3350°
620.5	2.00	0.3	COSPAR	42.2	47.1	–18.3193°
620.5	2.00	0.3	Revised COSPAR	45.6	50.2	–18.1877°
620.5	2.00	0.3	Viking I, Summer, Morning, Low Dust	43.2	47.9	–18.2836°
620.5	2.00	0.3	Viking I, Winter, Morning, Medium Dust	43.1	47.8	–18.2871°

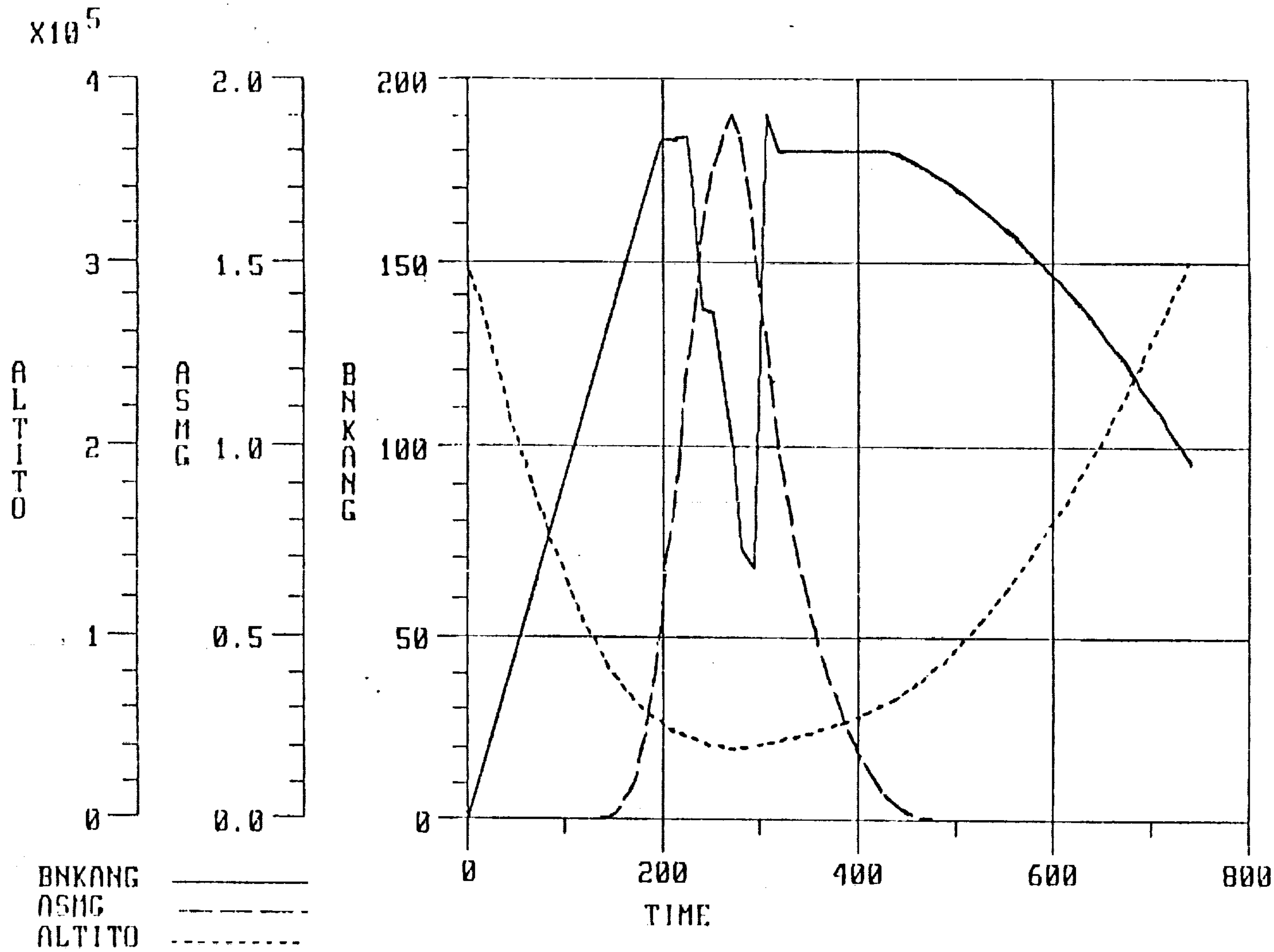

Figure 1. Typical time histories of altitude, acceleration and bankangle for blunt vehicle type 1 with L/D = .5 for maximum entry flight path angle.

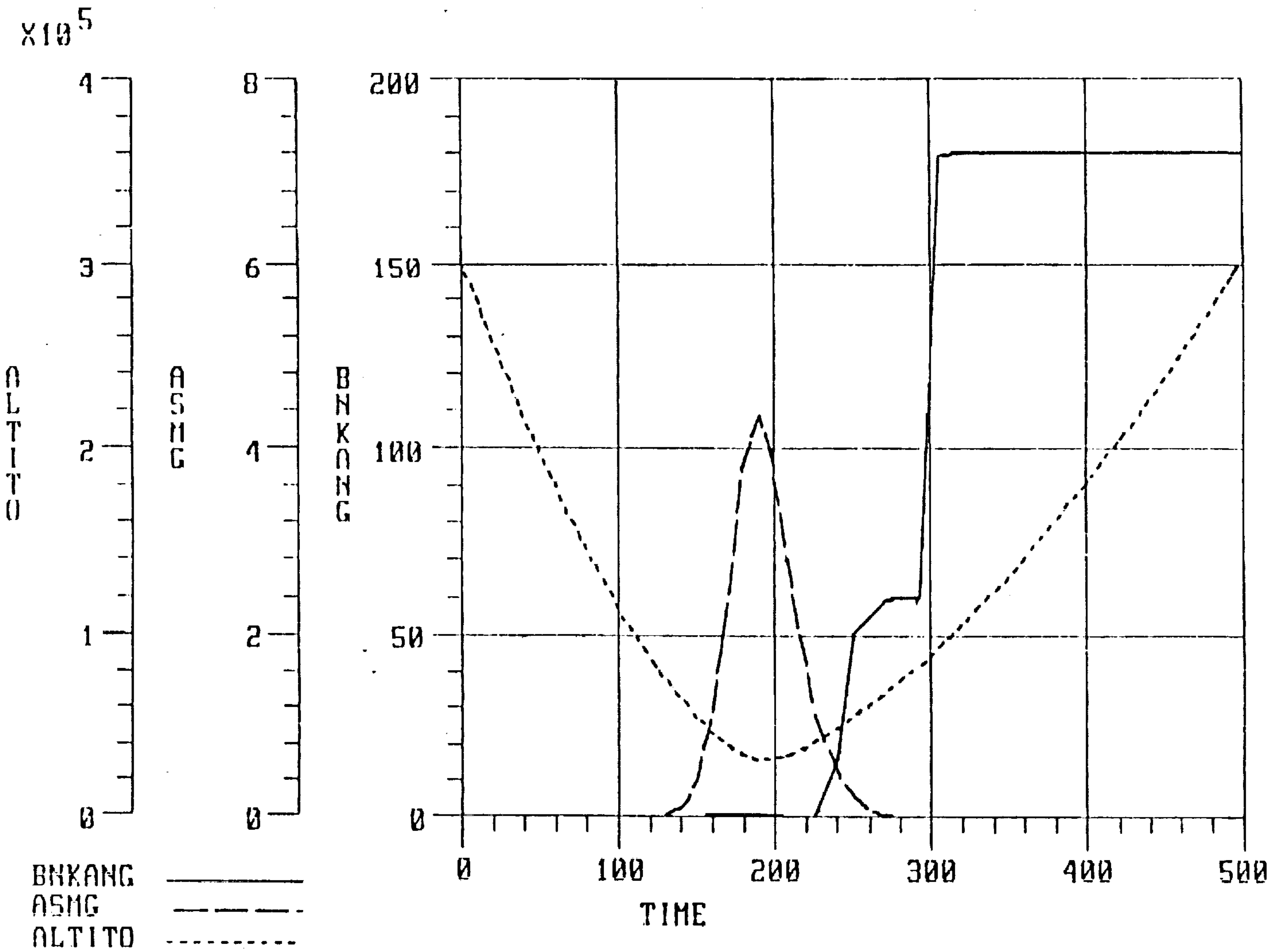

Figure 2. Typical time histories of bankangle, acceleration, and altitude for blunt vehicle type 1 with L/D - .5 for minimum entry flight path angle.

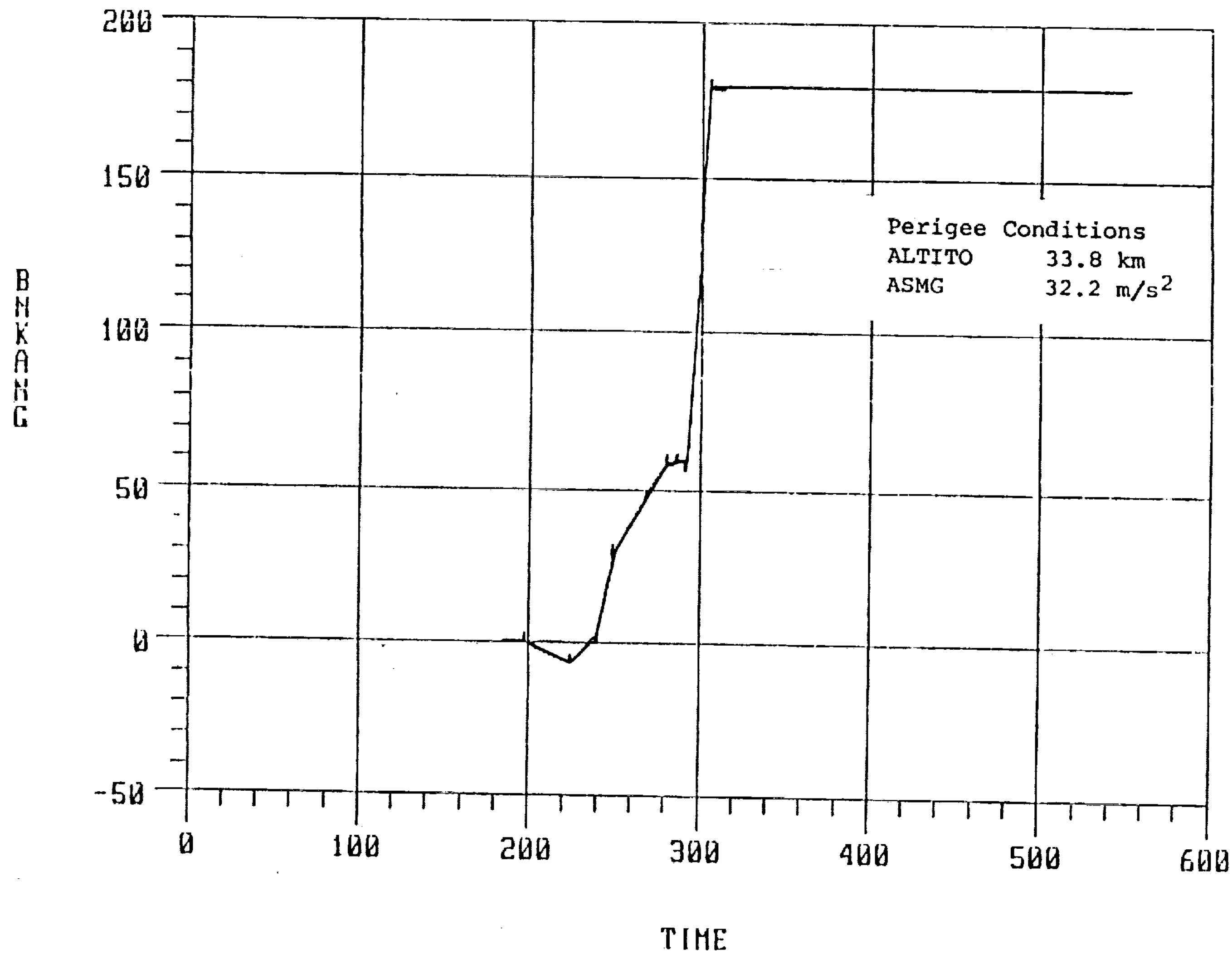

(a) Nine step bank profile

Figure 3. Bankangle time history for blunt vehicle type 1 with L/D = .3 for minimum flight path angle.

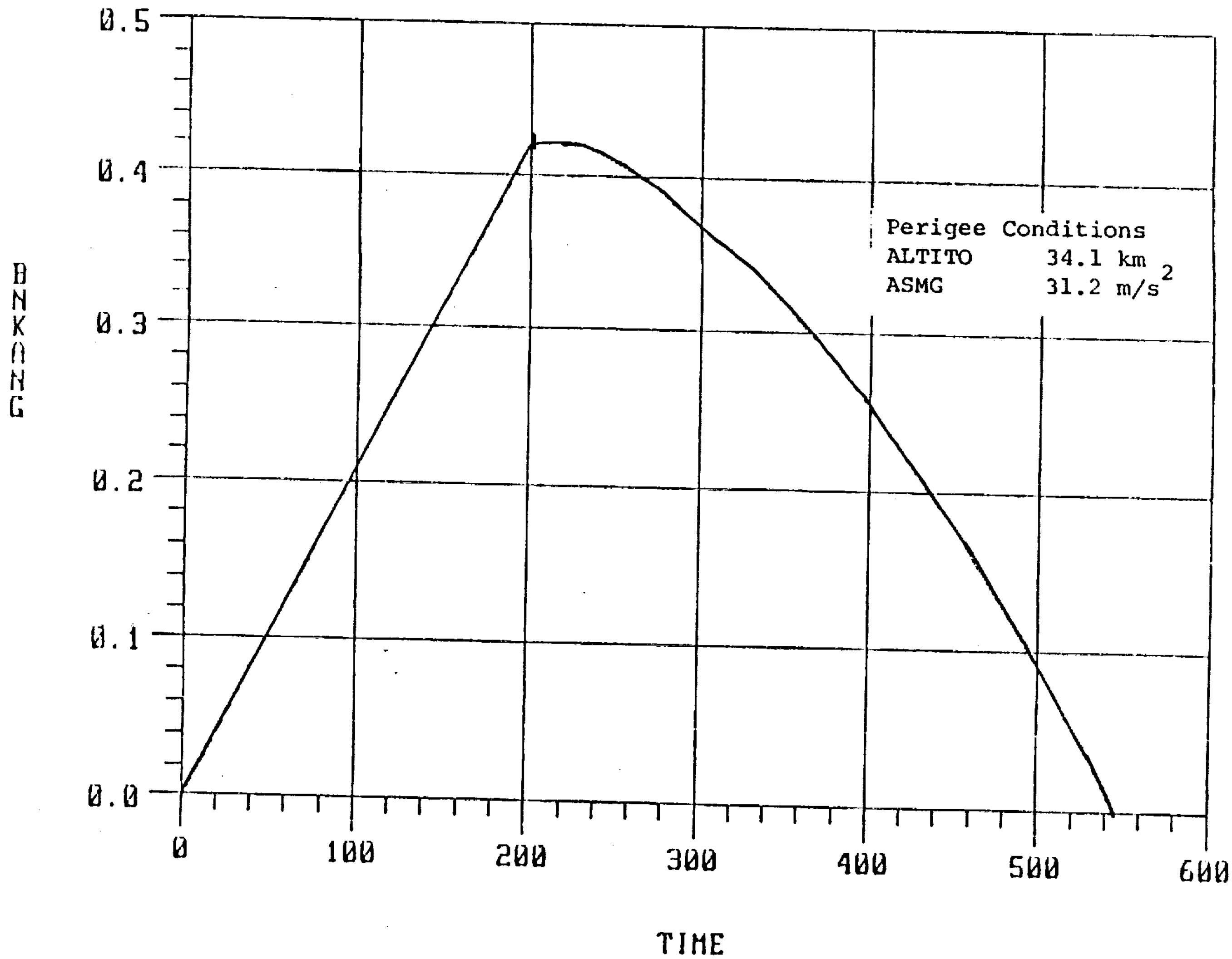

(b) Two step bank profile

Figure 3. Concluded.

NASA
National Aeronautics and Space Administration

Report Documentation Page

1. Report No. NASA TM-101669	2. Government Accession No.	3. Recipient's Catalog No.
4. Title and Subtitle: Aerobraking Characteristics for Several Potential Manned Mars Entry Vehicles		5. Report Date: November 1989
		6. Performing Organization Code
7. Author(s): Paul V. Tartabini and William T. Suit		8. Performing Organization Report No.
		10. Work Unit No. 506-46-21-01
9. Performing Organization Name and Address: NASA Langley Research Center, Hampton, VA 23665-5225		11. Contract or Grant No.
		13. Type of Report and Period Covered: Technical Memorandum
12. Sponsoring Agency Name and Address: National Aeronautics and Space Administration, Washington, DC 20546-0001		14. Sponsoring Agency Code

15. Supplementary Notes

16. Abstract

While a reduction in weight is always desirable for any space vehicle, it is crucial for vehicles to be used in the proposed Manned Mars Mission (MMM). One such way to reduce a spacecraft's weight is through aeroassist braking which is an alternative to retro-rockets, the traditional method of slowing a craft approaching from a high energy orbit. In this paper aeroassist braking was examined for two blunt vehicle configurations and one streamlined configuration. For each vehicle type, a range of lift-to-drag (L/D's) was examined and the entry angle windows, bank profiles, and trajectory parameters were recorded here. In addition, the sensitivities of velocity and acceleration with respect to the entry angle and bank angles were included. Also, the effect of using different atmosphere models was tested by incorporating several models into the simulation program.

17. Key Words (Suggested by Author(s)): Spacecraft Guidance; Aeroassist; Spacecraft Maneuvers; Manned Mars Mission	18. Distribution Statement: Unclassified - Unlimited; Subject Category 18

19. Security Classif. (of this report): Unclassified	20. Security Classif. (of this page): Unclassified	21. No. of pages: 28	22. Price: A03

 For sale by the National Technical Information Service, Springfield, VA 22161-2171